Water Air Soil Pollut (2024) 235:86
https://doi.org/10.1007/s11270-024-06895-y

Optimizing Microplastic Removal Through Coagulation-Sedimentation with Permanganate Pre-oxidation and Pre-chlorination

Haixuan Zhang · Haiyang Deng · Huase Ou · Ruijuan Liu · Yuheng Chen · Xinni Wu · Jianwei Fu

Received: 18 October 2023 / Accepted: 3 January 2024 / Published online: 15 January 2024

Abstract Improving the removal efficiency of microplastics (MPs) in water treatment plants is important to reduce their threats to the environment and human beings. In this study, the removal performance and mechanisms of MPs by pre-treatment-enhanced coagulation-flocculation-sedimentation (CFS) were evaluated. The sinking ratio of MPs was employed to quantify their removal efficiency in CFS, while zeta potentials and floc morphology were analyzed to understand the underlying mechanisms. Two key mechanisms for MP removal were identified: charge neutralization and sweep flocculation. As $KMnO_4$ pre-treatment was conducted, oxidation and MnO_2 attachment made the MP surface tend to interact with coagulants to form compact flocs. The removal efficiencies of 200-μm polyethylene terephthalate, polystyrene, and polyvinyl chloride increased 24%, 22%, and 17%, respectively, after $KMnO_4$ pre-treatment was performed. The increases were 38%, 40%, and 41%, respectively, for 6.5-μm ones. Notably, 6.5-μm polythene MPs seemed persistent in floating on the surface. Yet, chlorination pre-treatment contributed slight improvements. The intrinsic features of MPs, including density, size, hydrophobicity, and roughness, affected the basic removal in CFS. $KMnO_4$ oxidation and chlorination changed these features, promoting their interactions with coagulants and removal efficiencies. $KMnO_4$-enhanced CFS can be a potential treatment method for MP removal in water treatment plants.

Keywords Potassium permanganate · Chlorination · Coagulation · Microplastics

Highlights.
1. $KMnO_4$ pre-treatment promotes the removal efficiency of microplastics in coagulation.
2. $KMnO_4$ induces surface oxidation and MnO_2 attachment on microplastics.
3. $KMnO_4$ improves the interaction between microplastics and coagulants.
4. Chlorination presents no improvement in coagulation.
5. Improvements by $KMnO_4$ depend on the polymer type, size, hydrophobicity, and roughness.

Supplementary Information The online version contains supplementary material available at https://doi.org/10.1007/s11270-024-06895-y.

H. Zhang · H. Ou (✉) · R. Liu · Y. Chen · X. Wu · J. Fu
School of Environment, Guangdong Key Laboratory of Environmental Pollution and Health, Jinan University, Guangzhou 511443, China
e-mail: touhuase@jnu.edu.cn

H. Zhang
Ministry of Infrastructure, Jinan University, Guangzhou 510632, China

H. Deng
CECEP Construction Engineering Design Institute Limited Company, Chengdu 610052, China

H. Ou · R. Liu · Y. Chen
Center for Environmental Microplastics Studies, Jinan University, Guangzhou 511443, China

1 Introduction

Microplastic (MP) pollution has emerged as a pressing global environmental issue, with its presence observed in aquatic, terrestrial, and atmospheric environments. Of particular concern is the alarming contamination of freshwater bodies by MPs (Jian et al., 2020). Moreover, urban water management systems, including drinking water treatment plants (DWTPs) and wastewater treatment plants (WWTPs), are grappling with the challenges posed by MPs (Novotna et al., 2019). Research has verified that MPs can elicit toxic effects on various organisms, thereby posing significant threats to both aquatic and terrestrial ecosystems, as well as human health (Lett et al., 2021; Park et al., 2020). Given that the existing water treatment processes are not specifically designed to address MP particles, there is a critical need to develop efficient methods for the removal and control of MPs.

Traditional water treatment processes are the dominant contributors to MP removal in DWTPs and WWTPs (Hidayaturrahman and Lee, 2019; Lin et al., 2020). Among these processes, coagulation-flocculation-sedimentation (CFS) plays a crucial role in the elimination of MPs (Na et al., 2021), achieving removal rates ranging from 20 to 50% in DWTPs (Wang et al., 2020), and approximately 90% in WWTPs (Hidayaturrahman and Lee, 2019; Rajala et al., 2020). Lab-scale jar tests have been conducted to investigate the coagulation behavior and mechanisms involved in MP removal (Lu et al., 2021; Monira et al., 2021; Xue et al., 2021), with sweep flocculation being identified as the dominant mechanism in traditional CFS (Skaf et al., 2020). Moreover, the effectiveness of MP removal in CFS is influenced by their sizes and shapes (Zhang et al., 2020), as well as their inclusion in the background matrix (Xia et al., 2020). Furthermore, the weathering and aging degrees of MPs have been found to impact their removal efficiency during CFS (Lapointe et al., 2020). Understanding the behavior and mechanisms of MPs during coagulation is of paramount importance in improving the overall removal efficiency of MPs in water treatment processes.

To enhance the efficiency of CFS in removing microorganisms and organic matter, chemical pre-treatments have been investigated and implemented in both DWTPs and WWTPs. Common chemical pre-treatments include chlorination and potassium permanganate ($KMnO_4$) oxidation. These methods have shown success in inactivating aquatic microorganisms (Moradinejad et al., 2020) and oxidizing dissolved organic matter, thereby improving the removal efficiency of water treatment processes (Jian et al., 2019). However, it is important to note that while these pre-treatments may be effective for microorganisms and organic matter, their impact on microplastic removal may differ. Currently, only a limited number of studies have investigated the degradation and aging of microplastics resulting from these pre-treatments. Chlorination, for instance, has been observed to induce significant alterations in the chemical and physical characteristics of polypropylene, polyethylene (PE), and polystyrene (PS) (Kelkar et al., 2019). The fate and degradation mechanisms of microplastics under chlorination and $KMnO_4$ oxidation largely remain unexplored, and crucially, their effects on subsequent CFS for microplastic removal are still unknown. Exploring potential combinations of pre-treatments and CFS would hold significant value in developing effective treatment strategies for microplastics while minimizing their impact on human health and the environment.

This study aims to evaluate the removal performance and mechanisms of MPs in pre-treatment-enhanced CFS. MPs with different sizes and polymer types were selected as targets, while CFS conditions were explored and optimized. Furthermore, chlorination and $KMnO_4$ oxidation were tested. Subsequently, combination experiments of pre-treatments and coagulation jar tests were performed. The distribution status of MPs and the inherent mechanism involved in these combined treatments were explored.

2 Experimental

2.1 Materials

To obtain comparable results of surface characteristics before and after treatments, pure PE, polyethylene terephthalate (PET), PS, and polyvinyl chloride (PVC) particles were obtained from Zhonglian Plastic Ltd. (China). These MPs are frequently detected in water treatment processes. Furthermore, it has been found that small MPs (1–10 μm) were dominant in DWTPs and WWTPs (Rajala et al., 2020; Wang

et al., 2020). Thus, MP particles with mean diameters of 6.5 μm and 200 μm were both applied in this study. To perform contact angle analysis, MP sheets (5 mm × 5 mm, 1.5-mm thickness) were purchased from Goodfellow Cambridge Ltd. (UK). All MPs without treatment were preserved under a reductive atmosphere. An MP aging process was applied to improve the reality of the experiment (Section 2.2). Al-based polyaluminum chloride (PAC) coagulants and cationic polyacrylamide (PAM) were applied (Hidayaturrahman and Lee, 2019). NaClO solution (10% Cl), $KMnO_4$ (99.5%), PAC (98%), and cationic PAM (98%) were obtained from Macklin. Ultrapure water (18.2 MΩ) was used to prepare solutions. Lake water obtained from Jing Lake in Guangzhou was used as a background water matrix for pre-treatments and jar tests (Table S1). Before reaction, the lake water was filtered by a 0.22-μm membrane filter.

2.2 MP Aging and Characterization

To improve the reality assessments of water treatments, MPs were treated by aging before all experiments. Pristine MPs were sealed in a glass box with a customized glass cover (JGS-1) which can penetrate ultraviolet light (>95% UV-A in 360 nm). The box containing MPs was placed outdoors under natural sunlight irradiation for 60 days.

Basic characterization of MPs included morphology (scanning electron microscope, (SEM), FEI Apreo LoVac), chemical structure (Fourier transform infrared (FTIR) spectroscopy and X-ray photoelectron spectroscopy (XPS)), and surface physical features (roughness and contact angle). Detailed information is presented in Text S2.

2.3 Pre-treatments

Two pre-treatments, $KMnO_4$ oxidation and chlorination, were performed before coagulation. The lake water was used as the background matrixes. For each pre-treatment, the reaction time was set at 30 min. A concentration range of 0.4–10.0 mg L^{-1} $KMnO_4$ is applied in actual water treatment (Lin et al., 2013). In the current experiment, higher concentrations of $KMnO_4$ (2.5–100 mg L^{-1}) were used to obtain a more evident oxidation reaction. After MPs and $KMnO_4$ were added, the suspension was stirred at 30 rpm. For chlorination, a stock NaClO solution was prepared and added to the MP suspension to obtain the targeted concentration. Before chlorination experiments, the stock solution was diluted to a working dose, which was determined by Hach DPD powder pillows (2105569, 2105669). The concentration-time (*CT*) value was used to represent the chlorination dose. The reactions were conducted with *CT* values in the range of 75–3000 mg min L^{-1} (Office of Water, 1999).

Subsequently, two parts of experiments were conducted for the treated suspension. The first part was applied for the jar test. The suspension was moved to the jar test beakers, and the CFS process was performed. The second part was applied for characterization. MP particles were separated from the suspension and then washed with ultrapure water to remove the residual solution. The obtained MP particles were dried under 40 °C and applied for analysis.

2.4 Basic and Enhanced CFS Jar Tests

Coagulation processes were conducted using a jar test system (PB-900 programmable type) with six 1-L beakers. Two kinds of experiments were performed. Firstly, in the basic (sole) CFS experiment, the beakers were filled with 1 L background matrixes (lake water), and then a given amount (a final concentration of 10 mg L^{-1}) of aged MPs was added. The PAC concentration (10 mg L^{-1}) fell in the common PAC concentration range used in drinking water treatment (normally 5–20 mg L^{-1}). Some preliminary experiments had been performed, in which 2.5, 5, 10, and 20 mg L^{-1} PAC were applied in the jar test (data not included in this study). Secondly, in the enhanced combining experiment ($KMnO_4$ + CFS, or chlorination + CFS), the beakers were filled with 1 L pre-treated suspension which contained MPs (from the treated sample in Section 2.3). For both kinds of experiments, the zeta potential and MP sinking ratio were measured before reactions, and then stirrers were put into the suspension to perform mixing at 60 rpm for 2 min (the operational sequence is presented in Table S2). Subsequently, PAC was added, and a 60 rpm mixing (fast flocculation period) was conducted for 2 min. PAM was added at 1 min. After 1-min fast flocculation (300 rpm), a slow mixing period (10 min) was performed with 100 rpm stirring. The final stage was a 30-min settling. After the reaction, the zeta potential and MP sinking ratio were measured again. For each sample, at least three replications

were conducted to obtain the mean value and error bar.

2.5 Removal Efficiency Determination

As a particle sinks to the bottom of a vessel, it is considered to be removed by CFS. Thus, the sinking ratio of MPs can be set as their removal efficiency. After CFS, the supernatant liquid was removed, and the sinking MP flocs were obtained. A washing method was applied to obtain the MPs. Firstly, the sinking flocs were filtered by a 0.7-μm glass fiber filter. The filter, which contained MP flocs, was soaked in 1 M HCl solution for 24 h. After the flocs were disintegrated and coagulants were dissolved, the suspension (without a glass fiber filter) was filtered by 0.45 μm polytetrafluoroethylene filters. The MP particles were separated from flocs and dried before analysis. Detailed information on net MP mass determination can be found in our previous studies (Chen et al., 2022; Lin et al., 2022). The recovery rate of this method was tested to be 92–108% (Table S3).

2.6 Zeta Potential and Floc Morphology

The analysis methods of zeta potential and floc morphology are listed in Text S3.

2.7 Data Analysis/Statistics

One-way ANOVA (SPSS 19.0) was used to test the data of contact angle, MP mass, and sinking ratio. Data having $p < 0.05$ were considered significant.

3 Results and Discussion

3.1 Basic Removal of MPs in CFS

Before CFS, aged MPs exhibited distinct sinking behaviors (Fig. 1). Notably, the inherent sinking ratio of 200-μm PVC reached approximately 68%, while 6.5-μm PVC displayed a lower sinking ratio of around 35%. In contrast, aged PE MPs remained suspended on the water surface, owing to their different densities. PVC, with a higher density of approximately 1.4 g cm^{-3}, demonstrated a propensity to sink. Conversely, PE's density of 0.93 g cm^{-3} is lower than that of water, causing it to float undisturbed on the water surface.

Following the addition of the coagulant (PAC) and flocculation aids (cationic PAM) in CFS, the sinking ratio of MPs increased (Fig. 1, Table S4). Both PAC and cationic PAM concentrations were set as variables. Initially, sole PAC coagulation was conducted (with PAM concentration at 0, as shown in Fig. 1). For 10 mg L^{-1} MPs, the most effective removal efficiency was achieved with the addition of 10 mg L^{-1} PAC. For example, ~45% of 200-μm PET MPs were removed with 10 mg L^{-1} PAC, but this efficiency decreased to 37% when the PAC concentration was increased to 15 mg L^{-1}. Lower efficiencies were observed at PAC concentrations of 5 mg L^{-1} and 20 mg L^{-1}. Furthermore, the addition of cationic PAM further enhanced the removal efficiency. However, it appeared that the improvement in removal efficiency reached a limit as the PAM concentration increased. For example, the highest removal efficiency was observed for 200-μm PET with the combination of 10 mg L^{-1} PAC + 0.5 mg L^{-1} PAM, with no additional improvement observed as the PAM concentration was increased to 1 mg L^{-1}. A similar variation trend in removal efficiency was observed for smaller MPs, such as 6.5-μm PET. These findings suggested that appropriate concentrations of both the coagulant and flocculation aid should be carefully selected based on the given MP concentration.

The removal of MPs in the basic CFS jar test varied significantly based on the polymer types of MPs. For 200-μm PE, only limited removal was observed (< 5%). The removal of 6.5-μm PE remained at 0 even as the PAM concentration increased, which can be attributed to its low-density nature. The flocs containing PE MPs were challenging to sink due to their overall densities being lower than that of water. In contrast, a high removal was achieved for PVC. Generally, the order of removal efficiency when combining CFS with PAC and PAM followed PVC > PET > PS > PE, which was associated with the densities and basic sinking ratios of these four types of MPs. The most significant improvements in removal (from inherent sinking ratio to the highest removal in CFS) were observed for 200-μm PET, PS, and PVC, with increases of 38%, 17%, and 17%, respectively. For 6.5-μm PET, PS, and PVC, the improvements were 44%, 12%, and 25%, respectively. These findings indicate that the intrinsic features of MPs, such as density,

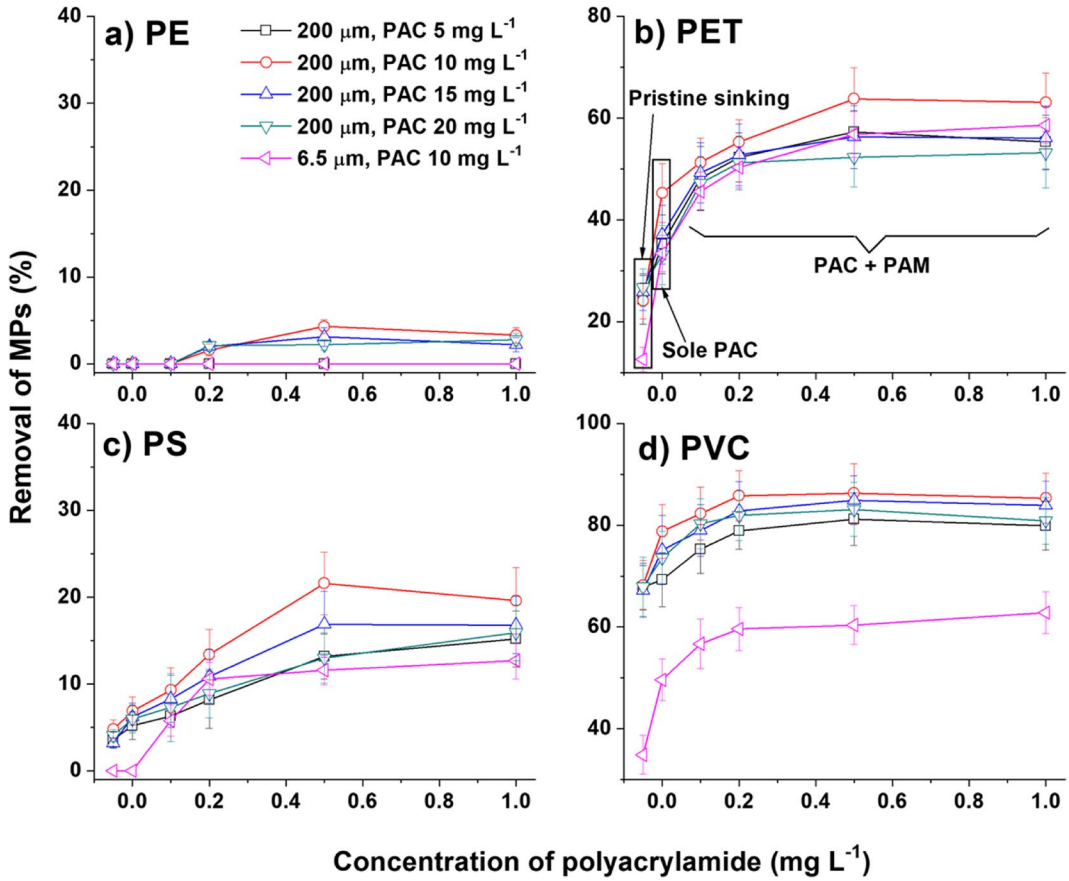

Fig. 1 Removal of MPs in basic CFS jar test. Jar test conditions: background matrix pH = 6.69, polyaluminum chloride 5–20 mg L^{-1}, cationic polyacrylamide 0–1.0 mg L^{-1}, reaction temperature 25 °C. Sizes of MPs are 200 μm and 6.5 μm

size, and sinking ratio, play a vital role in determining their basic removal. Coagulation processes can effectively improve the sinking ratio of all MPs, especially those with higher densities.

3.2 Enhanced CFS with Pre-treatments

$KMnO_4$ oxidation and chlorination can enhance the efficiency of CFS. In the experiments conducted, the conditions for CFS were set as 10 mg L^{-1} PAC and 0.5 mg L^{-1} cationic PAM, with other reaction parameters detailed in Table S2.

The enhanced sinking ratios of MPs are presented in Figs. 2 and S2 and Table S5. When the $KMnO_4$ pre-treatment was induced, the efficiency of CFS was further improved. Taking 200-μm PET as an example, the sinking ratio (removal) increased from 64 to 88% after 10 mg L^{-1} $KMnO_4$ oxidation + CFS, and this level was maintained even with higher $KMnO_4$ concentrations. Similar tendencies were observed for PE (increased by ~22%) and PS (increased by ~21%). Notably, significant promotions were also confirmed, with increases of ~40% and ~41%, respectively, for 6.5-μm PET and PS. However, the removal of PE remained zero under all treatments. As for 200-μm PVC, with its basic removal already exceeding 80%, $KMnO_4$ pre-oxidation seemed to have only a slight effect on it. Surprisingly, the removal of 6.5-μm PVC increased from 60 to 100%, indicating a substantial enhancement. Generally, an appropriate addition concentration of 10 mg L^{-1} $KMnO_4$ was found to be effective.

On the other hand, chlorination resulted in only minor improvements (Fig. S2). Enhanced CFS after chlorination showed increased removal for PET and PS, while no variation was observed for PE and PVC.

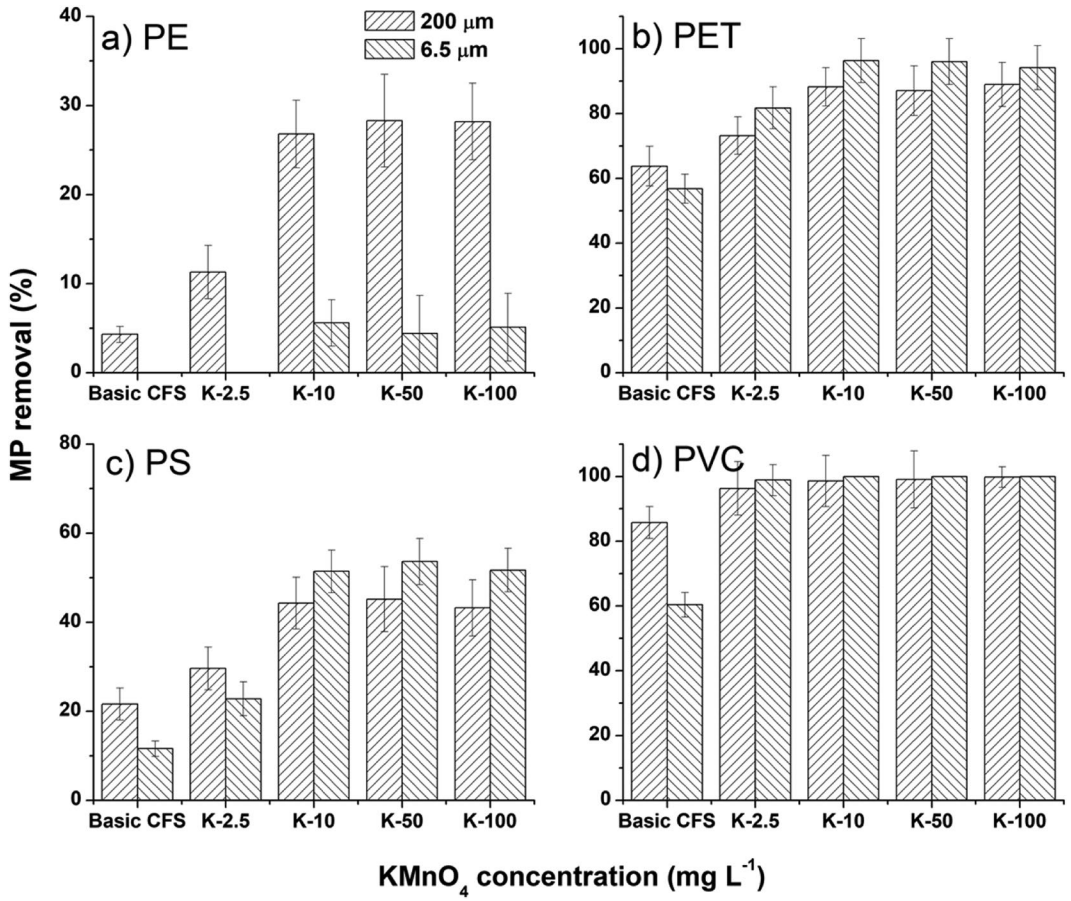

Fig. 2 Removal of MPs in $KMnO_4$-enhanced CFS jar test. $KMnO_4$ oxidation experiment: $[KMnO_4]_0$ = 2.5, 10, 50, and 100 mg L^{-1}; reaction time = 30 min; reaction temperature 25 °C; the sizes of MPs are 200 μm and 6.5 μm. Jar test conditions: background matrix pH = 6.73, polyaluminum chloride 10 mg L^{-1}, cationic polyacrylamide 0.5 mg L^{-1}, reaction temperature 25 °C

3.3 Zeta Potential

The zeta potential of particles plays a crucial role in the formation and sedimentation of flocs. When the zeta potential is reduced to a range of low values, typically from −10 to 10 mV, it facilitates the formation of compact flocs. This condition leads to more rapid and efficient flocculation, primarily driven by charge neutralization. Figure 3 shows the zeta potential variations in basic and enhanced CFS. The control group represented the original zeta potential of raw water. Following CFS, the zeta potential values were reduced to a range of ±10 mV, indicating a feasible destabilization condition. Upon the application of $KMnO_4$ oxidation, the zeta potential approached zero more closely. In comparison, the improvement achieved through chlorination was relatively slight when compared to that of $KMnO_4$ oxidation. These findings suggested that $KMnO_4$ oxidation pre-treatment promoted charge neutralization, leading to the improved formation of compact flocs in the presence of MPs. However, this effect was not observed with chlorination. Additionally, the enhancement appeared to be more efficient for smaller MPs (6.5 μm), exhibiting smaller absolute zeta potential values under the same reaction conditions.

3.4 Floc Morphology

The formation morphology of flocs is important to evaluate the CFS. Figure 4 shows the flocs of MPs after basic and enhanced CFS. Due to the random

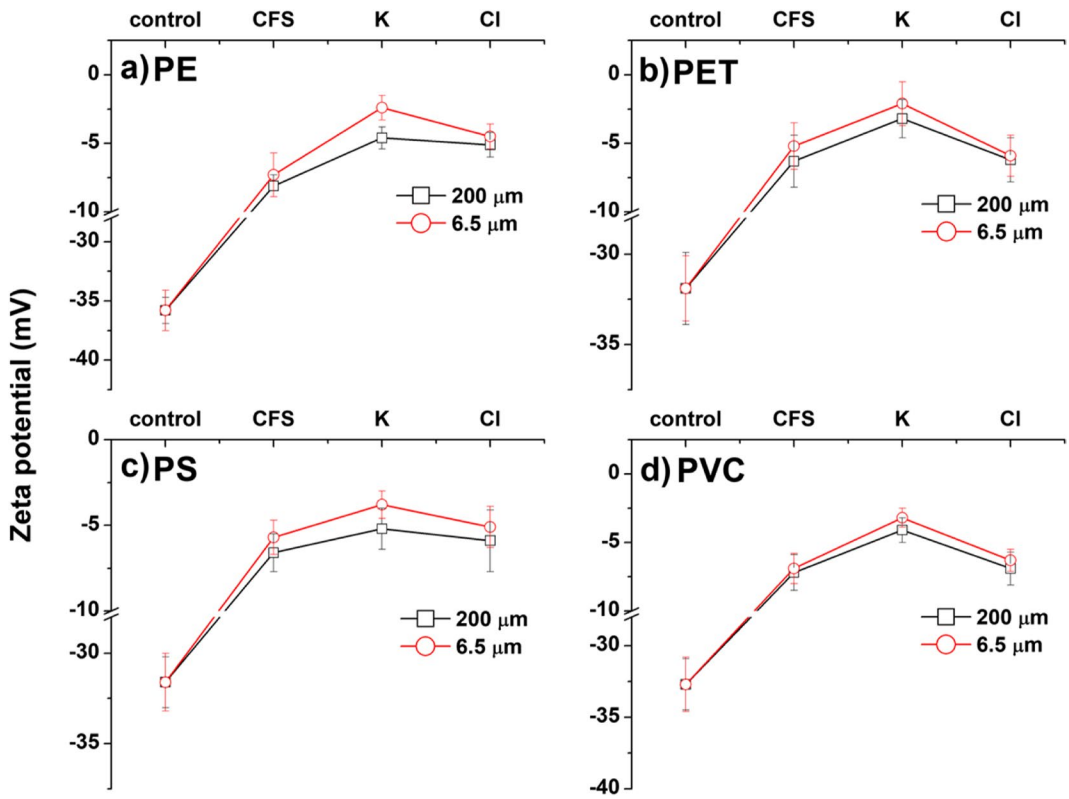

Fig. 3 Variation of zeta potential. $KMnO_4$ oxidation experiment: $[KMnO_4]_0$ = 10 mg L^{-1}, reaction time = 30 min. Chlorination experiment: CT = 75 mg min L^{-1}, reaction temperature 25 °C, the sizes of MPs are 200 μm and 6.5 μm. Jar test conditions: background matrix pH = 6.73, polyaluminum chloride 10 mg L^{-1}, cationic polyacrylamide 0.5 mg L^{-1}, reaction temperature 25 °C. Control indicates the background water matrix. CFS indicates the sole coagulation-flocculation-sedimentation treatment. K indicates $KMnO_4$ oxidation–enhanced CFS. Cl indicates chlorination-enhanced CFS

and irregular nature of floc formation, only qualitative observations were discussed. After basic CFS, all MPs were encapsulated within loose and bondless flocs formed by polymer coagulants.

In contrast, after $KMnO_4$ + CFS, the flocs exhibited a darker color with more visible interspaces, indicating a more compact structure than those formed during basic CFS. The presence of additional voids within these compact flocs implied enhanced aggregation, increasing their density and leading to faster sedimentation. The removal results (Fig. 2) further supported this deduction. On the other hand, for chlorination + CFS, the flocs appeared similar to those in sole CFS, without any noticeable improvement in aggregation. Consequently, low removal efficiencies were observed when chlorination was applied.

Furthermore, the average size (d_{50}) of flocs was measured (Table S6). In basic CFS, the floc sizes of 200-μm MPs were in the range of 288–364 μm, and they increased significantly in the $KMnO_4$ + CFS experiment. For example, the one of PVC rose to 867 ± 66 μm, nearly three times that in a single CFS. Again, the improvement by chlorination was weaker. These findings further supported the conclusion that $KMnO_4$ oxidation can enhance the formation of MP flocs during CFS.

3.5 MP Morphology Variation After Oxidation and Chlorination

Intact surfaces were observed for the aged MPs with different polymer types. Among these MPs, PE exhibited a coil-like surface, while the other three MPs had smooth layer-shaped surfaces. These differences may be attributed to variations in their production and polymerization processes.

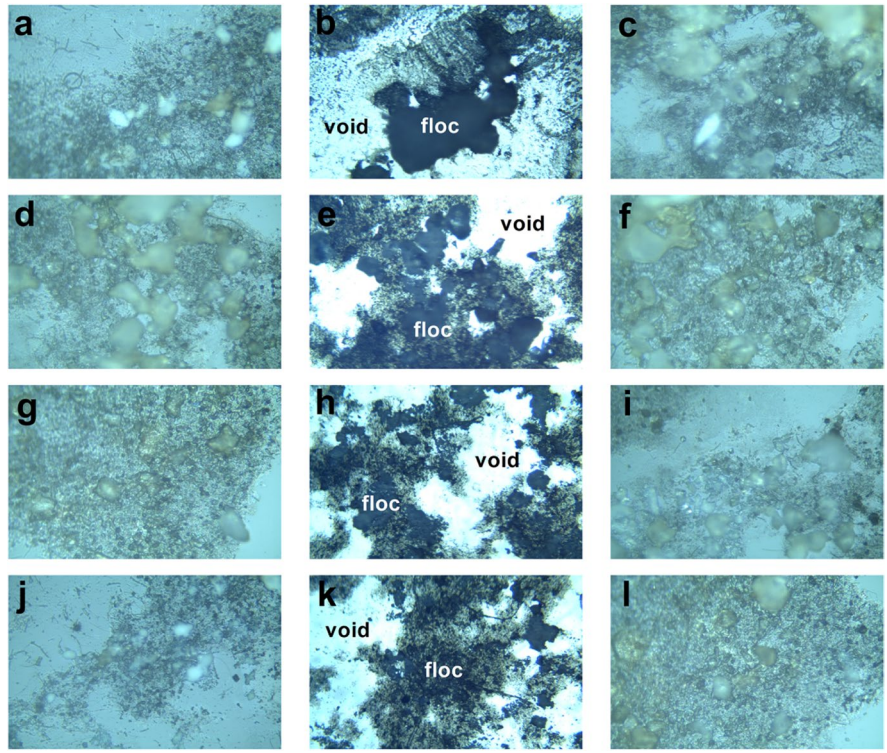

Fig. 4 Images of flocs in jar tests: **a** PE in CFS, **b** PE in $KMnO_4$ + CFS, **c** PE in chlorination + CFS, **d** PET in CFS, **e** PET in $KMnO_4$ + CFS, **f** PET in chlorination + CFS, **g** PS in CFS, **h** PS in $KMnO_4$ + CFS, **i** PS in chlorination + CFS, **j** PVC in CFS, **k** PVC in $KMnO_4$ + CFS, and **l** PVC in chlorination + CFS. $KMnO_4$ oxidation experiment: $[KMnO_4]_0 = 10$ mg L^{-1}, reaction time = 30 min. Chlorination experiment: $CT = 75$ mg min L^{-1}, reaction temperature 25 °C, the size of MPs is 6.5 µm. Jar test conditions: background matrix pH = 6.73, polyaluminum chloride 10 mg L^{-1}, cationic polyacrylamide 0.5 mg L^{-1}, reaction temperature 25 °C

Theoretical surface modifications on MPs include oxidation destruction and the attachment of nano-MnO_2. In the current experiment, only slight surface destruction was observed (Fig. 5). Some wrinkles and cracks appeared on the surfaces of PET and PVC, but no destruction on the other two polymers. Interestingly, small adhesive substances were evident on all MPs, possibly indicating the presence of nascent-state nano-MnO_2. These modifications could affect the surface hydrophobicity and roughness of MPs. In comparison to our previous study (Chen et al., 2022), these modifications were relatively weak, likely due to the low concentration (10 mg L^{-1}) of $KMnO_4$ applied in this study. This concentration is more representative of actual water treatment scenarios, which typically use concentrations of 1–5 mg L^{-1}. Consequently, it can be concluded that the observed modifications in this study reflected the real-life situations of MPs after $KMnO_4$ oxidation.

On the other hand, chlorination resulted in evident destruction and corrosions on the surfaces of PET, PS, and PVC. Notably, massive wrinkles appeared on PET and PS, while pores covered the surface of PE and PVC, indicating distinct destruction processes and mechanisms on different polymers. The dominant mechanism for PET and PS involved the disconnection of high polymer valence linkages, leading to layer-shaped wrinkles. Conversely, for PVC, corrosion seemed to occur first, followed by the detachment of tiny particles from the main MP bodies, eventually forming small pores.

3.6 Chemical Variations of MPs

FTIR can determine the chemical composition characteristics on the surface and depths of several millimeters in the MPs. Some new characteristic peaks appeared on the surface of MPs treated by $KMnO_4$ oxidation and chlorination (Fig. S3), mainly in the ranges of 2500–2800 cm^{-1} and 3000–3500 cm^{-1}. The characteristic peaks in these intervals are related to the oxidation bonds, including O–H, C–O, and C=O. For PS, a markedly broad peak appeared in the range of 2500–2800 cm^{-1}, while PET exhibited a broad peak in the range of 3000–3500 cm^{-1}. These results indicated the generation of oxidized functional groups on the surface of MPs after $KMnO_4$ oxidation and chlorination.

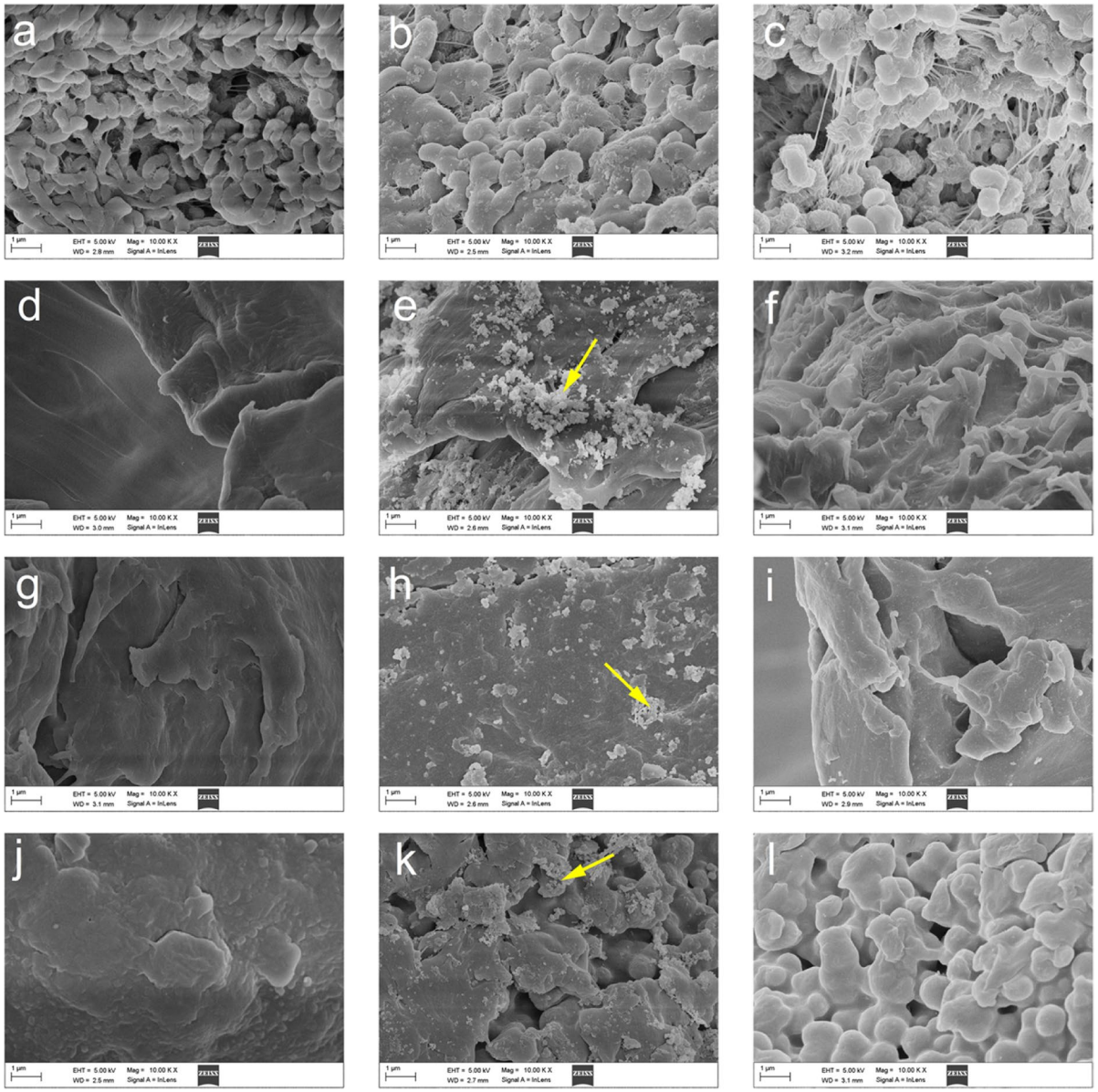

Fig. 5 SEM images of MPs: **a** aged PE, **b** PE after $KMnO_4$ treatment, **c** PE after chlorination treatment, **d** aged PET, **e** PET after $KMnO_4$ treatment, **f** PET after chlorination treatment, **g** aged PS, **h** PS after $KMnO_4$ treatment, **i** PS after chlorination treatment, **j** aged PVC, **k** PVC after $KMnO_4$ treatment, and **l** PVC after chlorination treatment. $KMnO_4$ oxidation experiment: $[KMnO_4]_0 = 10$ mg L^{-1}, reaction time = 30 min. Chlorination experiment: $CT = 75$ mg min L^{-1}, reaction temperature 25 °C, the size of MPs is 200 µm. Arrows indicate the MnO_2 particles on MP surfaces

XPS measurements were conducted to evaluate the chemical valence bond variations of MPs (Fig. 6). Only a few oxidized functional groups were found on the aged MPs. The O 1s spectrum of aged PET demonstrated a high intensity (Fig. 6b), attributed to its inherent O–C and O=C structures. After $KMnO_4$ oxidation, oxygen-related bonds on the MP surfaces increased, evident from the higher intensity of the O 1s spectrum for all polymers. After deconvolution (Fig. 6e), three sub-peaks were identified, namely, O–C (531.6 eV), O=C (532.9 eV), and O–Mn (529.8 eV) bonds. The O–C and O=C sub-peaks implied

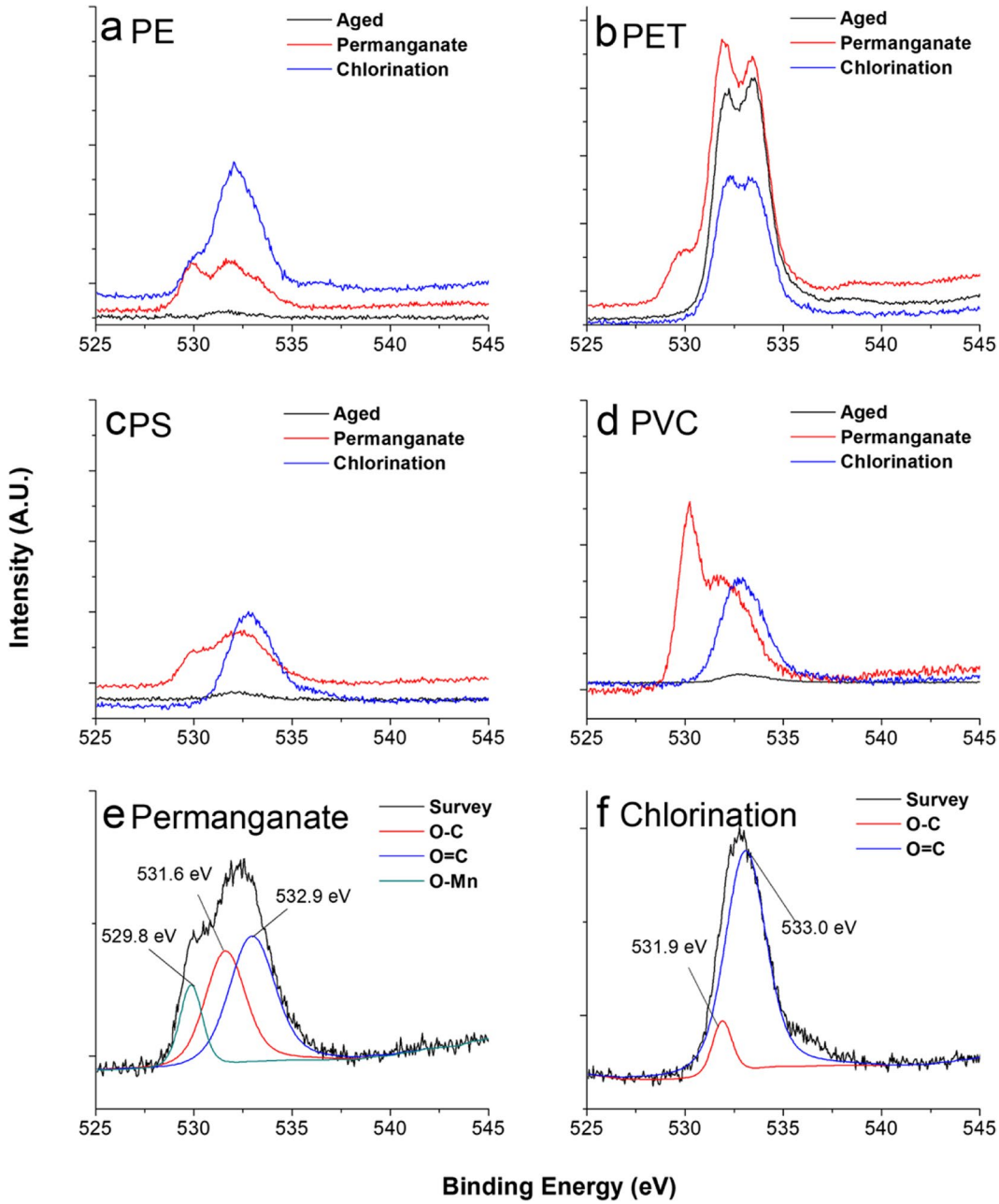

Fig. 6 X-ray photoelectron spectroscopy (oxygen) variations of MP particles: **a** PE, **b** PET, **c** PS, **d** PVC, **e** O 1s parent peak and deconvolution sub-peaks of PET after $KMnO_4$ oxidation, and **f** O 1s parent peak and deconvolution sub-peaks of PET after chlorination. $KMnO_4$ oxidation experiment: $[KMnO_4]_0$ = 10 mg L^{-1}, reaction time = 30 min. Chlorination experiment: dose CT = 75 mg min L^{-1}, reaction temperature 25 °C, the size of MPs is 200 µm

oxidation on the MP surfaces, while the O–Mn sub-peak indicated the generation of MnO_2, confirming that the nano-particles on MP surfaces were MnO_2 adhering after $KMnO_4$ treatment.

After chlorination, the intensity of the O 1s spectrum for all MPs increased similarly, but the overall characteristic peak centered around 532.5 eV (Fig. 6f). After deconvolution, O–C (531.6 eV) and

O=C (532.9 eV) sub-peaks were identified, but no O–Mn (529.8 eV), suggesting MP surfaces were also oxidized during chlorination. The Cl 2p spectrum increased after chlorination, indicating the generation of chlorinated functional groups. The organic framework of the polymer surfaces underwent chlorination mainly due to addition and substitution reactions after bond cleavage. After deconvolution, two sub-peaks were observed, representing Cl 2p1 (202.1 eV) and Cl 2p3 (200.4 eV), respectively (Fig. S4e). Of note, a certain peak was observed in the Cl 2p spectrum of aged PVC (Fig. S4d) due to the existence of chlorine in its skeleton. After chlorination, the intensity of Cl 2p increased significantly, especially in PVC, indicating a stronger affinity between PVC and chlorine. Consequently, PVC was more susceptible to corrosion, which was also confirmed by SEM results revealing evident corrosion on the surface of PVC.

3.7 Roughness, Hydrophobicity, and Mechanisms

Surface roughness and hydrophobicity can significantly affect the interactions between MPs and coagulants. Roughness differed by polymer type. The roughness of aged PET, PS, and PVC was < 0.1 μm, but the one of PE was higher (Table S7). Aged PE had a gully surface (Fig. 5), contributing to roughness at 0.364 μm.

After $KMnO_4$ oxidation and chlorination, the roughness of all MPs increased. Although the increase in roughness of PE seemed implicit due to its high initial value, the increases for the other three polymers were significant. For example, the roughness of PVC rose from 0.026 to 0.264 μm (~1000%). SEM images of aged PVC showed a smooth surface, but abundant pores with MnO_2 particles were observed after $KMnO_4$ oxidation (Fig. 5), consistent with the roughness results. Chlorination also led to the formation of pore canals on PVC, contributing to an increase in roughness to 0.163 μm (a rise of ~600%). Similar variations in roughness were observed for PS and PET. The roughness of PET increased by ~900% (after $KMnO_4$ oxidation) and ~800% (after chlorination), supported by SEM images showing relevant results. This increased roughness facilitated the access and interaction of coagulants with MPs, thereby enhancing coagulation and sedimentation (Lapointe et al., 2020).

The hydrophobicity of MP surface can be reflected by the contact angle. The contact angles of aged MPs were all > 80°, indicating that they were all hydrophobic (Table S8). After treatments, the contact angles decreased for all MPs. Significant variations were observed for PET, PS, and PVC, while only a slight decrease was noted for PE. $KMnO_4$ oxidation induced more dramatic decreases than chlorination. For example, the contact angle of PVC declined from 85.6 to 21.9° and 18.3° after low-dose and high-dose $KMnO_4$ oxidation, respectively. This could be attributed to the generation of C–O and C=O bonds and the attachment of MnO_2. However, after chlorination, the contact angle only decreased to 63.3° and 46.2°, suggesting a weaker destruction of hydrophobicity. This declining hydrophobicity also facilitated the interaction between the coagulant and MPs, leading to improved coagulation.

3.8 Enhanced Mechanism and Economic Cost

The above results indicated that the dominant mechanism for basic MP removal included charge neutralization (decreasing zeta potential) and sweep flocculation (formation of MP flocs), which was consistent with the previous research (Skaf et al., 2020). When $KMnO_4$ pre-oxidation was induced, it oxidized the surface of MPs, which increased the roughness and reduced hydrophobicity. These characteristic variations improve the adsorption and interaction of coagulants with MPs, enhancing the sweep flocculation process. Furthermore, the presence of nascent-state MnO_2 promotes the interaction between coagulants and MPs, leading to the formation of denser flocs. The attachment of MnO_2 compresses the electric double layer around MPs, facilitating coagulation. All these processes contribute to the improved removal of MPs in enhanced CFS by $KMnO_4$ pre-oxidation.

On the other hand, chlorination only induced weak improvements in charge neutralization and sweep flocculation. Chlorination causes some destruction on PET and PS, increasing their hydrophilicity. This led to increased adsorption of coagulants on these two MPs, which benefited coagulation. In contrast, only slight destruction was observed for PE and PVC, resulting in minimal improvements in removal.

At a dosage concentration of 10 mg L^{-1} $KMnO_4$, the removal rates of various MPs were significantly improved. If the $KMnO_4$ concentration increased,

the improvement of MP removal rate was insignificant. Therefore, 10 mg L^{-1} $KMnO_4$ was used to calculate the economic cost. The cost of adding 10 mg L^{-1} $KMnO_4$ was 0.168 RMB m^{-3} (the price of solid $KMnO_4$ was 16,800 RMB ton^{-1} in Sep. 2023). This cost accounts for a small proportion of the overall cost of drinking water (5–7 RMB m^{-3} in China). Moreover, $KMnO_4$ pre-oxidation not only is targeted at MPs, but also can improve the removal and purification of other pollutants and microorganisms. Therefore, the cost of using $KMnO_4$ pre-oxidation to improve the removal rate of MPs would be acceptable.

Both $KMnO_4$ pre-oxidation and pre-chlorination can improve the removal rate of MPs; $KMnO_4$ pre-oxidation especially is highly effective. However, the actual economic costs of these two methods need to be further determined based on the actual water treatment process and water quality requirements. The concentration of MPs added in this experiment is higher than that in actual water treatment, and the natural raw water body contains various other pollutants and microorganisms. In the actual treatment process, $KMnO_4$ pre-oxidation and pre-chlorination are often used as pre-treatment methods for microorganisms and organic matter. While treating these pollutants, they also remove MPs. Taking into account the effects and costs of the two pre-treatments, $KMnO_4$ pre-oxidation is an effective and economically feasible method to improve the MP removal rate.

4 Conclusion

The removal of MPs in basic CFS can be considered to assist their sinking ratios. Charge neutralization and sweep flocculation were fundamental mechanisms that were further boosted by $KMnO_4$ pre-oxidation. Oxidation and MnO_2 attachment induced by $KMnO_4$ made the MP surfaces more inclined to interact with coagulants, leading to the formation of compact flocs and ultimately improving the removal efficiency. Yet, chlorination pre-treatment only contributed slightly to this improvement.

The intrinsic characteristics of MPs, such as density, size, hydrophobicity, and roughness, all play significant roles in their basic removal in CFS. Furthermore, $KMnO_4$ oxidation and chlorination can alter these characteristics, thereby affecting their removal efficiencies in CFS. For example, the removal efficiencies of 6.5-μm PET, PS, and PVC increased by 38%, 40% and 41%, respectively, after $KMnO_4$ pre-treatment was performed. Using $KMnO_4$-enhanced CFS could be a potential treatment method for MPs with different sizes and polymer types.

Author Contribution H. Ou and H. Zhang: conceived and designed the experiments. H. Zhang, R. Liu, and Y. Chen: carried out the experiment. H. Ou, H. Zhang, and H. Deng: cowrote the paper. X. Wu: provided constructive suggestions for the manuscript revision. J. Fu: provided constructive suggestions for results and discussion. All authors participated in the discussion.

Funding This project is supported by the National Natural Science Foundation of China (Grant No. 42377373) and Southern Marine Science and Engineering Guangdong Laboratory (Zhuhai) (No. SML2021SP208).

Data Availability Relevant data sources are cited in the text and, where applicable, listed in the bibliography.

Declarations

Competing Interests The authors declare no competing interests.

References

Chen, Y., Liu, R., Wu, X., Liu, Y., Fu, J., & Ou, H. (2022). Surface characteristic and sinking behavior modifications of microplastics during potassium permanganate pre-oxidation. *Journal of Hazardous Materials, 422*, 126855.

Hidayaturrahman, H., & Lee, T. G. (2019). A study on characteristics of microplastic in wastewater of South Korea: Identification, quantification, and fate of microplastics during treatment process. *Marine Pollution Bulletin, 146*, 696–702.

Jian, M. F., Zhang, Y., Yang, W. J., Zhou, L. Y., Liu, S. L., & Xu, E. G. (2020). Occurrence and distribution of microplastics in China's largest freshwater lake system. *Chemosphere, 261*, 128186.

Jian, Z. Y., Bai, Y. H., Chang, Y. Y., Liang, J. S., & Qu, J. H. (2019). Removal of micropollutants and cyanobacteria from drinking water using KMnO4 pre-oxidation coupled with bioaugmentation. *Chemosphere, 215*, 1–7.

Kelkar, V. P., Rolsky, C. B., Pant, A., Green, M. D., Tongay, S., & Halden, R. U. (2019). Chemical and physical changes of microplastics during sterilization by chlorination. *Water Res., 163*, 114871.

Lapointe, M., Farner, J. M., Hernandez, L. M., & Tufenkji, N. (2020). Understanding and improving microplastic removal during water treatment: Impact of coagulation and flocculation. *Environmental Science & Technology, 54*, 8719–8727.

Lett, Z., Hall, A., Skidmore, S., & Alves, N. J. (2021). Environmental microplastic and nanoplastic: Exposure routes and effects on coagulation and the cardiovascular system. *Environ. Pollut., 291*, 118190.

Lin, J., Wu, X., Liu, Y., Fu, J., Chen, Y., & Ou, H. (2022). Sinking behavior of polystyrene microplastics after disinfection. *Chemical Engineering Journal, 427*, 130908.

Lin, J., Yan, D., Fu, J., Chen, Y., & Ou, H. (2020). Ultraviolet-C and vacuum ultraviolet inducing surface degradation of microplastics. *Water Research, 186*, 116360.

Lin, T., Pan, S., Chen, W., & Bin, S. (2013). Role of pre-oxidation, using potassium permanganate, for mitigating membrane fouling by natural organic matter in an ultrafiltration system. *Chem. Eng. J., 223*, 487–496.

Lu, S., Liu, L. B., Yang, Q. X., Demissie, H., Jiao, R. Y., An, G. Y., & Wang, D. S. (2021). Removal characteristics and mechanism of microplastics and tetracycline composite pollutants by coagulation process. *Science of the Total Environment, 786*, 147508.

Monira, S., Bhuiyan, M. A., Haque, N., & Pramanik, B. K. (2021). Assess the performance of chemical coagulation process for microplastics removal from stormwater. *Process Safety and Environmental Protection, 155*, 11–16.

Moradinejad, S., Trigui, H., Maldonado, J. F. G., Shapiro, J., Terrat, Y., Zamyadi, A., Dorner, S., & Prevost, M. (2020). Diversity assessment of toxic cyanobacterial blooms during oxidation. *Toxins, 12*, 728.

Na, S. H., Kim, M. J., Kim, J. T., Jeong, S., Lee, S., Chung, J., & Kim, E. J. (2021). Microplastic removal in conventional drinking water treatment processes: Performance, mechanism, and potential risk. *Water Res., 202*, 117417.

Novotna, K., Cermakova, L., Pivokonska, L., Cajthaml, T., & Pivokonsky, M. (2019). Microplastics in drinking water treatment - Current knowledge and research needs. *Science of the Total Environment, 667*, 730–740.

Office of Water, U (1999) Combined sewer overflow technology fact sheet chlorine disinfection, in U. Office of Water (Ed.)Washington, D.C., United States Environmental Protection Agency.

Park, J. W., Lee, S. J., Hwang, D. Y., & Seo, S. (2020). Recent purification technologies and human health risk assessment of microplastics. *Materials, 13*, 5196.

Rajala, K., Gronfors, O., Hesampour, M., & Mikola, A. (2020). Removal of microplastics from secondary wastewater treatment plant effluent by coagulation/flocculation with iron, aluminum and polyamine-based chemicals. *Water Res., 183*, 116045.

Skaf, D. W., Punzi, V. L., Rolle, J. T., & Kleinberg, K. A. (2020). Removal of micron-sized microplastic particles from simulated drinking water via alum coagulation. *Chem. Eng. J., 386*, 123807.

Wang, Z. F., Lin, T., & Chen, W. (2020). Occurrence and removal of microplastics in an advanced drinking water treatment plant (ADWTP). *Sci. Total Environ., 700*, 134520.

Xia, Y., Xiang, X. M., Dong, K. Y., Gong, Y. Y., & Li, Z. J. (2020). Surfactant stealth effect of microplastics in traditional coagulation process observed via 3-D fluorescence imaging. *Sci. Total Environ., 729*, 138783.

Xue, J. K., Peldszus, S., Van Dyke, M. I., & Huck, P. M. (2021). Removal of polystyrene microplastic spheres by alum-based coagulation-flocculation-sedimentation (CFS) treatment of surface waters. *Chem. Eng. J., 422*, 130023.

Zhang, Y. L., Diehl, A., Lewandowski, A., Gopalakrishnan, K., & Baker, T. (2020). Removal efficiency of micro- and nanoplastics (180 nm-125 mu m) during drinking water treatment. *Sci. Total Environ., 720*, 137383.